WATER STRUCTURE

Reversible structural transformations in supercooled liquid water from 135 to 245 K

Loni Kringle*, Wyatt A. Thornley*, Bruce D. Kay†, Greg A. Kimmel†

A fundamental understanding of the unusual properties of water remains elusive because of the limited data at the temperatures and pressures needed to decide among competing theories. We investigated the structural transformations of transiently heated supercooled water films, which evolved for several nanoseconds per pulse during fast laser heating before quenching to 70 kelvin (K). Water's structure relaxed from its initial configuration to a steady-state configuration before appreciable crystallization. Over the full temperature range investigated, all structural changes were reversible and reproducible by a linear combination of high- and low-temperature structural motifs. The fraction of the liquid with the high-temperature motif decreased rapidly as the temperature decreased from 245 to 190 K, consistent with the predictions of two-state "mixture" models for supercooled water in the supercritical regime.

Water has many anomalous properties compared with "simple" liquids (*1*–*3*). These anomalies, which are related to temperature-dependent changes in the hydrogen-bonding network [for example, (*4*)], are typically enhanced in supercooled water. However, no consensus has emerged on whether the changes arise from several structurally distinct components in the liquid or from a unimodal, continuous distribution of structures (*2*–*7*). Models that have been developed to explain water's properties include the liquid-liquid critical point (LLCP) scenario (*8*, *9*) and the singularity-free scenario (*10*). The main difficulty in determining which of the models is correct is the limited data in the relevant temperature, T, and pressure, P, ranges. For water at ambient pressures, which is the focus of this work, data are largely missing from 160 to 235 K ("no man's land") because of rapid crystallization of the supercooled liquid (*2*, *3*). Whether rapid crystallization is just an experimental obstacle or a fundamental problem signaling the inability of water to thermally equilibrate before crystallization is also a major unanswered question (*9*, *11*, *12*).

We used infrared (IR) spectroscopy to investigate the structural transformations of transiently heated, supercooled water with nanosecond time resolution. Because of the high cooling rates for the experiments and the low temperature at which all of the IR spectra were obtained, the results were related to the "inherent structure" of water as determined in molecular dynamics (MD) simulations (*3*, *6*, *13*). The results show that water relaxed from its initial configuration to a steady-state configuration before the onset of crystallization for the experimentally accessible temperature range (135 K < T < 245 K). These structural changes were reversible over the full temperature range. Finally, water's inherent structure could be reproduced by a linear combination of two structural motifs corresponding to the liquid hyperquenched from high temperatures and water isothermally annealed at the glass transition temperature, T_g (≈136 K). These results provided support for the hypothesis that supercooled water at low pressure can be described as a mixture of two, structurally distinct components from 135 to 245 K (*6*, *9*, *14*–*23*).

Water films with typical thicknesses of ~15 nm were adsorbed on Pt(111) or graphene/Pt(111) in ultrahigh vacuum at 70 K and then heated at ~10^{10} K/s with nanosecond laser pulses (Fig. 1A) (*24*, *25*). For each heat pulse, $T(t)$, the films spent ~3 ns near the maximum temperature, T_{max}, before rapidly cooling to the base temperature (Fig. 1B). The changes in water's structure were monitored with IR spectroscopy. The results should be representative of bulk water and not strongly influenced by the nanoscale thickness of the films (supplementary text, section A).

Figure 1C shows the evolution of the IR spectra in the OH-stretch region for water films prepared with different initial configurations and then heated to T_{max} = 215 K. Isothermally annealing the water films at or near T_g for ~100 s produced films with an IR spectrum characteristic of low-density amorphous ice (LDA) (*2*, *3*) (plot a in Fig. 1C, blue line). Pulsed heating to high temperatures produced films with a different characteristic IR spectrum: plot a in Fig. 1C shows an example for a film heated to 297 K for three pulses (red line). The IR spectrum of crystalline ice (CI) is also shown for comparison (plot a in Fig. 1C, black line). Because the IR spectra were sensitive to the hydrogen-bonding configuration of the water molecules (*23*, *26*, *27*), these spectra indicated that there were substantial structural differences between the three films. We refer to water films prepared by pulsed heating to 297 K as "hyperquenched water" (HQW). For the experiments reported below, the initial configuration of the water was either LDA or HQW.

After heating the water to 215 K, the IR spectra evolved as the number of heat pulses, N_p, increased (plots b and c in Fig. 1C and fig. S1). For both LDA and HQW, the spectra observed just before the onset of measurable crystallization (e.g., N_p = 670) were the same

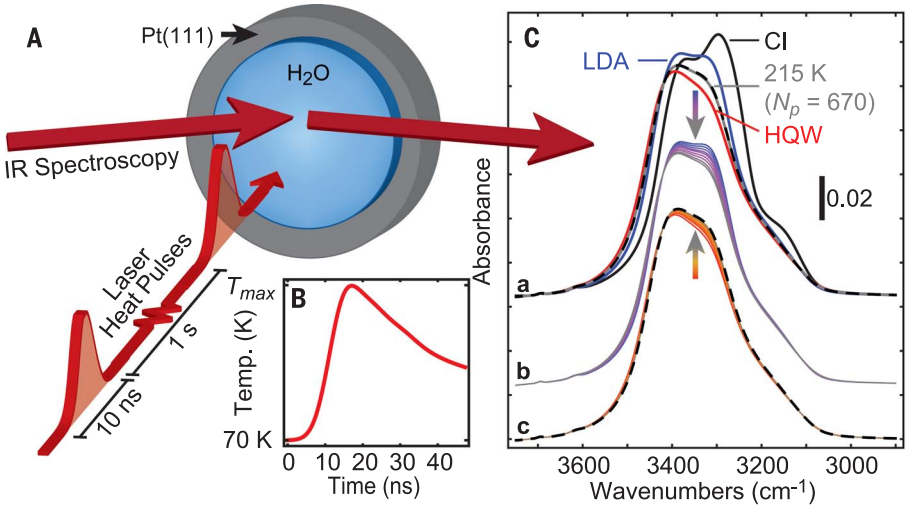

Fig. 1. Experimental approach and IR spectra. (**A**) Schematic of transiently heating nanoscale water films adsorbed on Pt(111) [or graphene/Pt(111)]. (**B**) Calculated temperature (Temp.) versus time, $T(t)$, during a typical heat pulse. (**C**) IR spectra of transiently heated, 50-monolayer water films on graphene/Pt(111) measured at 70 K. In plot a, spectra for HQW, LDA, and CI are all distinct. In plot b, LDA was heated to 215 K for N_p = 4, 10, 19, 31, 55, 100, 210, and 670. In plot c, HQW was heated to 215 K for N_p = 1, 2, 4, 7, 31, 100, and 670. For plots b and c, the arrows indicate the increasing N_p.

Physical Sciences Division, Pacific Northwest National Laboratory, P.O. Box 999, Richland, WA 99352, USA.
*These authors contributed equally to this work.
†Corresponding author. Email: gregory.kimmel@pnnl.gov (G.A.K.); bruce.kay@pnnl.gov (B.D.K.)

(plot a in Fig. 1C, gray and dashed black lines). Further pulsed heating ultimately led to crystallization of the water films (fig. S2). Similar evolution of the IR spectra was observed for a wide range of pulsed-heating temperatures (170 K ≤ T_{max} ≤ 260 K). In all cases, the IR spectra of the transiently heated water could be reproduced by a linear combination of the LDA, HQW, and CI spectra, and the mole fraction of LDA, HQW, and CI (f_{LDA}, f_{HQW}, and f_{CI}, respectively) in the water film could be determined (*25*).

Figure 2 shows f_{LDA}, f_{HQW}, and f_{CI} versus N_p for T_{max} = 215 K. For HQW and LDA, f_{HQW} asymptotically approached ~0.64 before crystallization (solid and open circles). Similarly, f_{LDA} approached ~0.36 (solid and open squares). Evolution of water's structure from LDA or HQW to a common intermediate structure was also observed for other temperatures (e.g., fig. S3). An assumption of the current approach is that transiently heating water multiple times near T_{max} produced the same structural changes that would be observed versus time in an isothermal experiment (supplementary text, section B).

The pulsed-heating experiments allowed water films to be brought into the supercooled region multiple times. Thus, changing T_{max} during an experiment allowed us to explore the reversibility of the structural changes in the transiently heated water films. Figure 3A shows f_{HQW} and f_{LDA} versus N_p where T_{max} was repeatedly cycled between 215 K for 100 pulses and 252 K for 10 pulses (a subset of the corresponding IR spectra is shown in fig. S4). The key observation is that each time T_{max} changed, the structure quickly evolved toward a new steady-state configuration characteristic of that temperature.

Reversible structural changes were also observed for water when the temperature was cycled between 135 K (isothermal heating for 130 s) and 215 K (pulsed heating for 1 ≤ N_p ≤ 400) (Fig. 3B and fig. S4B). Because of the slower relaxation kinetics for LDA compared with HQW, more heat pulses were required to approach the steady-state configuration in that case. As a result, the onset for crystallization occurred after only two temperature cycles in Fig. 3B (black triangles). However, for both experiments, the structural changes seen at 215 K could be reversed by simply changing the temperature. More examples of reversible structural transformations for supercooled water at other temperatures are shown in fig. S5. The results in Figs. 1 to 3 show that the observed changes in the water are not irreversible structural transformations associated with crystallization (*11*) or crossing a spinodal (*1*). The characteristic relaxation times for HQW and LDA compared with ice nucleation and growth rates at T_{max} = 215 K are discussed in the supplementary text, section C.

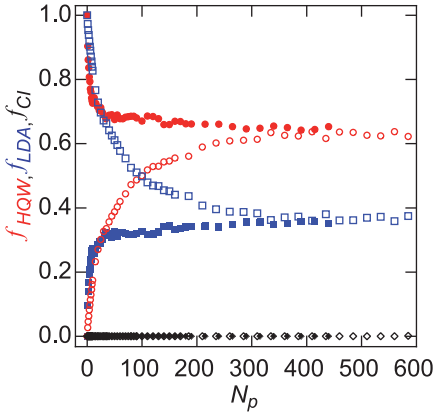

Fig. 2. Structural relaxation for HQW and LDA. f_{HQW} (circles), f_{LDA} (squares), and f_{CI} (diamonds) versus N_p for T_{max} = 215 K and initial configuration of either LDA (open symbols) or HQW (solid symbols).

The results suggest that the (quenched) IR spectra observed just before crystallization reflected the steady-state structure of water at T_{max}. The steady-state spectra, $S(T_{max}, \omega)$, could all be fit as linear combinations of the HQW and LDA spectra [$S_{HQW}(\omega)$ and $S_{LDA}(\omega)$, respectively] (fig. S6):

$$S(T_{max}, \omega) = f^{SS}_{HQW}(T_{max}) \cdot S_{HQW}(\omega) + f^{SS}_{LDA}(T_{max}) \cdot S_{LDA}(\omega)$$

where ω is the frequency and f^{SS}_{HQW} (f^{SS}_{LDA}) is the fraction of the water corresponding to HQW (LDA) at steady state. Figure 4A shows $f^{SS}_{HQW}(T_{max})$ (circles) determined from the average of measurements of several individual experiments with LDA and HQW films on both Pt(111) and graphene/Pt(111) at each temperature (fig. S7). The red line shows a fit to the data using the logistic function (*23*)

$$f^{SS}_{HQW}(T) = \{1 + \exp[-(T - T_0)/\Delta T]\}^{-1}$$

with T_0 = 210 ± 3 K and ΔT = 8.5 K. For T_{max} ≤ 170 K, the steady-state IR spectra of the transiently heated water films do not change (figs. S8 and S9), indicating that water over a wide temperature range has essentially the same structure as LDA.

Two-component models propose that water at ambient pressure is an inhomogeneous liquid with regions of higher density and entropy [a high-density liquid (HDL)] and lower density and entropy [a low-density liquid (LDL)] (*6*, *16*, *19*, *22*). The ability to decompose the steady-state IR spectra of supercooled water into a linear combination of two components is consistent with these models, as were the differences between the HQW and LDA spectra, which indicated a higher proportion of local tetrahedral configurations in LDA (*26*, *27*). IR spectra calculated from classical MD simulations at supercooled temperatures also agreed qualitatively with the IR spectra presented here (*26*).

The observation that f^{SS}_{HQW} was ~1 for T_{max} > 245 K was probably related to the rapid structural equilibration of mildly supercooled water and the experiment's finite cooling rate. At high temperatures, water maintained its equilibrium structure near T_{max}. However, as the sample cooled, the relaxation rate slowed to the point where the structural changes could not keep up, quenching the film. Thus, the structural information from temperatures above ~245 K was lost as the samples cooled. Although HQW was probably a mixture of HDL and LDL (*2*, *3*), the experiments did not allow us to unambiguously determine its composition. Furthermore, reported values for $f_{HDL}(T)$ vary substantially, which made it difficult to decide which, if any, of these could be used to assign the composition of HQW (supplementary text, section D, and figs. S10 and S11). By contrast, we assume that LDA was essentially 100% LDL because it was prepared by annealing at T_g.

Previous experiments that used x-ray, Raman, and IR spectroscopy and the optical Kerr effect have shown bimodal characteristics for water above the homogeneous nucleation temperature

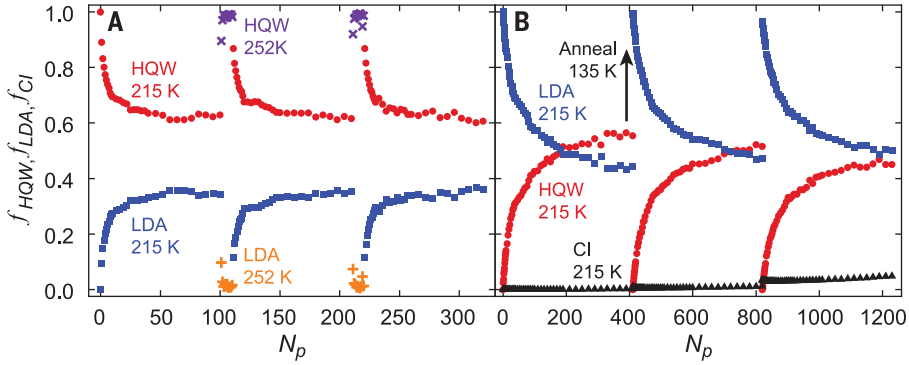

Fig. 3. Reversible structural transformations. (**A** and **B**) $f_{HQW}(N_p)$ and $f_{LDA}(N_p)$ for pulse-heating at (A) T_{max} = 215 and 252 K or (B) T_{max} = 215 K and isothermal annealing at 135 K. The red circles and purple ×'s show f_{HQW} for T_{max} = 215 and 252 K, respectively. The blue squares and orange crosses show f_{LDA} for T_{max} = 215 and 252 K, respectively. In (B), f_{CI} (black triangles) is also shown.

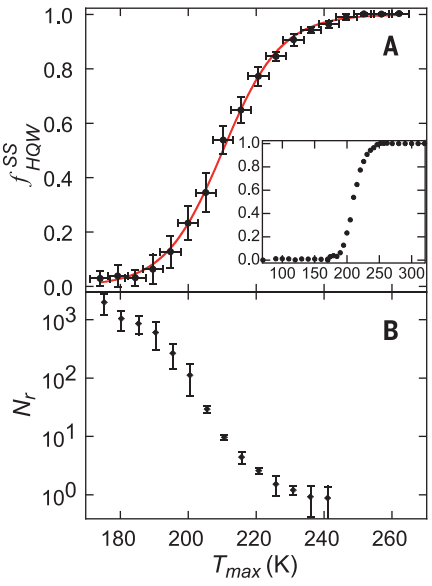

Fig. 4. Steady-state structure and relaxation rates. (**A**) f^{SS}_{HQW} versus T_{max} (black circles). The vertical error bars show 1 SD for the measured values, whereas the horizontal error bars arise from uncertainty in the laser power. A logistic function (red line) fits the data. The inset shows $f^{SS}_{HQW}(T_{max})$ over a wider temperature range. (**B**) Characteristic number of pulses to relax HQW, N_r, versus T_{max}.

(~235 K) (*17*, *18*, *28*, *29*). Our results were qualitatively consistent with these experiments. However, because all of the IR spectra reported here were measured at the same temperature, $T_{measure}$ = 70 K, the observed changes were not caused by thermal effects associated with measurements made at different temperatures (*30*). Instead, the quenched state reflected the structure of water at T_{max}, but with reduced thermal broadening because of the low temperature for the IR measurements. Thus, our results correspond to the "inherent structures" obtained from MD simulations where the systems were instantaneously quenched to 0 K (*3*, *6*, *13*) (supplementary text, section E).

The characteristic number of heat pulses, N_r, for water to relax was determined by fitting f_{HQW} with a stretched exponential function (eq. S2). Figure 4B shows N_r for experiments with HQW. For T_{max} > 240 K, N_r could not be determined because there was little change in the structure. At lower temperatures, N_r rapidly increased from ~1 at T_{max} = 236 K to ~2000 at T_{max} = 175 K. The structural relaxation time, τ_{rel}, was estimated by multiplying N_r by a characteristic duration for the heat pulses, δt_{pulse} ~ 3 ns (*25*). This suggests that τ_{rel} increased from ~3 ns to 6 μs as T_{max} decreased from 236 to 175 K. The rapid increase in N_r (or τ_{rel}) is consistent with MD simulations (*31*, *32*) and experiments on confined water (*3*).

The experiments reported here focused on water's relaxation before crystallization. To fully crystallize the films would have taken much longer (fig. S2), particularly for T_{max} < 215 K, and was not explored in detail. An earlier report, which investigated the ice nucleation rate in transiently heated water films, followed the crystallization to completion for T_{max} ≥ 212 K (*33*). For 50-monolayer films, the number of pulses required to crystallize 50% of those films, N_{xtal}, were 4040, 2560, 1240, and 890 for T_{max} = 212, 216, 219, and 226 K, respectively. For the experiments shown in fig. S2, N_{xtal} was 2580 and 2050 for LDA and HQW, respectively, which was comparable to the earlier results.

Two-component models generally predict that water's structure changes rapidly only at intermediate temperatures, with comparatively slower changes at high and low temperatures, at which the structure is dominated by HDL-like and LDL-like species, respectively (fig. S10) (*3*, *16*, *22*, *31*). Previous experiments, including x-ray scattering (*34*) and Raman spectroscopy (*29*), suggest that the high-temperature, HDL-dominated region extends down to ~245 K (fig. S11), whereas the structure of water changes more rapidly at lower temperatures (*18*, *20*). The onset of rapid changes in water's structure indicated by x-ray scattering approximately corresponds to the temperature below which the transiently heated films became sensitive to the structure (Fig. 4A). Therefore, we expect that $f^{SS}_{HQW}(T_{max})$ reflects the structural changes in water in the temperature range where it is changing rapidly, particularly at temperatures below 230 K, for which there are few existing data. However, because of the finite cooling rate in the experiments, $f^{SS}_{HQW}(T_{max})$ does not directly correspond to the fraction of HDL-like species versus (isothermal) temperature, $f_{HDL}(T)$.

In the LLCP scenario, the Widom line is the locus of maxima in the correlation length as a function of temperature and pressure in the one-phase region (*14*). At ambient pressure, $f_{HDL}(T)$ is changing the most rapidly at the Widom line (*3*, *31*). For micrometer-scale liquid drops, x-ray scattering data place the Widom line, T_{WL}, at 229 K (*20*). Although the midpoint for $f^{SS}_{HQW}(T_{max})$ is at 210 ± 3 K (Fig. 4A), we expect the results on transiently heated water films to be shifted to lower temperatures relative to $f_{HDL}(T)$ because of the effects of the finite cooling rate (supplementary text, section D). Figure S12 shows an example in which $f^{SS}_{HQW}(T_{max})$ is compared with the inherent structures obtained from MD simulations (*13*). We also note that the rapid heating and cooling in the current experiments could potentially favor different structures from those measured in the liquid drops where the cooling rate was low enough that the water maintained its equilibrium structure as it cooled (supplementary text, section B). Nonetheless, the experiments on transiently heated nanoscale water films provide previously unreported data that are needed to test, validate, and refine various postulates advanced to explain water's anomalous properties.

REFERENCES AND NOTES

1. R. J. Speedy, *J. Chem. Phys.* **86**, 982–991 (1982).
2. O. Mishima, H. E. Stanley, *Nature* **396**, 329–335 (1998).
3. P. Gallo *et al.*, *Chem. Rev.* **116**, 7463–7500 (2016).
4. F. H. Stillinger, *Science* **209**, 451–457 (1980).
5. J. D. Smith *et al.*, *Proc. Natl. Acad. Sci. U.S.A.* **102**, 14171–14174 (2005).
6. A. Nilsson, L. G. M. Pettersson, *Nat. Commun.* **6**, 8998 (2015).
7. A. K. Soper, *J. Chem. Phys.* **150**, 234503 (2019).
8. P. H. Poole, F. Sciortino, U. Essmann, H. E. Stanley, *Nature* **360**, 324–328 (1992).
9. J. C. Palmer *et al.*, *Nature* **510**, 385–388 (2014).
10. S. Sastry, P. G. Debenedetti, F. Sciortino, H. E. Stanley, *Phys. Rev. E* **53**, 6144–6154 (1996).
11. D. T. Limmer, D. Chandler, *J. Chem. Phys.* **135**, 134503 (2011).
12. E. B. Moore, V. Molinero, *Nature* **479**, 506–508 (2011).
13. K. T. Wikfeldt, A. Nilsson, L. G. M. Pettersson, *Phys. Chem. Chem. Phys.* **13**, 19918–19924 (2011).
14. L. Xu *et al.*, *Proc. Natl. Acad. Sci. U.S.A.* **102**, 16558–16562 (2005).
15. F. Mallamace *et al.*, *Proc. Natl. Acad. Sci. U.S.A.* **104**, 424–428 (2007).
16. V. Holten, M. A. Anisimov, *Sci. Rep.* **2**, 713 (2012).
17. A. Taschin, P. Bartolini, R. Eramo, R. Righini, R. Torre, *Nat. Commun.* **4**, 2401 (2013).
18. J. A. Sellberg *et al.*, *Nature* **510**, 381–384 (2014).
19. J. Russo, H. Tanaka, *Nat. Commun.* **5**, 3556 (2014).
20. K. H. Kim *et al.*, *Science* **358**, 1589–1593 (2017).
21. L. P. Singh, B. Issenmann, F. Caupin, *Proc. Natl. Acad. Sci. U.S.A.* **114**, 4312–4317 (2017).
22. R. Shi, J. Russo, H. Tanaka, *Proc. Natl. Acad. Sci. U.S.A.* **115**, 9444–9449 (2018).
23. N. J. Hestand, J. L. Skinner, *J. Chem. Phys.* **149**, 140901 (2018).
24. Y. Xu, N. G. Petrik, R. S. Smith, B. D. Kay, G. A. Kimmel, *Proc. Natl. Acad. Sci. U.S.A.* **113**, 14921–14925 (2016).
25. Materials and methods are available as supplementary materials.
26. Y. Ni, J. L. Skinner, *J. Chem. Phys.* **145**, 124509 (2016).
27. B. M. Auer, J. L. Skinner, *J. Chem. Phys.* **128**, 224511 (2008).
28. Y. Maréchal, *J. Mol. Struct.* **1004**, 146–155 (2011).
29. Q. Sun, *Chem. Phys. Lett.* **568-569**, 90–94 (2013).
30. P. L. Geissler, *J. Am. Chem. Soc.* **127**, 14930–14935 (2005).
31. E. B. Moore, V. Molinero, *J. Chem. Phys.* **130**, 244505 (2009).
32. D. T. Limmer, D. Chandler, *Faraday Discuss.* **167**, 485–498 (2013).
33. G. A. Kimmel *et al.*, *J. Chem. Phys.* **150**, 204509 (2019).
34. C. Benmore, L. C. Gallington, E. Soignard, *Mol. Phys.* **117**, 2470–2476 (2019).

ACKNOWLEDGMENTS

Funding: This work was supported by the U.S. Department of Energy (DOE), Office of Science, Basic Energy Sciences, Chemical Sciences, Geosciences, and Biosciences Division. This research was performed by using EMSL, a national scientific user facility sponsored by DOE's Office of Biological and Environmental Research and located at the Pacific Northwest National Laboratory, which is operated by Battelle for the DOE. **Author contributions:** The research was designed and supervised by G.A.K. and B.D.K. L.K. and W.A.T. conducted the experiments. L.K., W.A.T., and G.A.K. analyzed the data. L.K. and G.A.K. wrote the manuscript, with input from all authors. **Competing interests:** None declared. **Data and materials availability:** All data are available in the main text or the supplementary materials.

SUPPLEMENTARY MATERIALS

science.sciencemag.org/content/369/6510/1490/suppl/DC1
Materials and Methods
Supplementary Text
Figs. S1 to S17
References (*35*–*53*)

16 March 2020; accepted 28 July 2020
10.1126/science.abb7542

Reversible structural transformations in supercooled liquid water from 135 to 245 K

Loni Kringle, Wyatt A. Thornley, Bruce D. Kay and Greg A. Kimmel

Science **369** (6510), 1490-1492.
DOI: 10.1126/science.abb7542

Supercooled water structures

Water displays a number of anomalous properties that are further enhanced in its supercooled state, but experimental studies at ambient pressure must obtain data before the onset of rapid crystallization at temperatures below ~240 kelvin. Kringle *et al.* obtained infrared spectra of supercooled water films at temperatures between 135 and 235 kelvin that formed for a few nanoseconds by ultrafast heating and cooling. Supercooled water thermally equilibrates before crystallization above 170 kelvin, and over the range of temperatures studied, the structure of water was shown to be a linear combination of a high-density and a low-density liquid.

Science, this issue p. 1490